IMPROVED UNDERSTANDING OF RECOMBINATION AT THE Si/Al$_2$O$_3$ INTERFACE

F. Werner[1], B. Veith[1], D. Zielke[1], L. Kühnemund[2], C. Tegenkamp[2], M. Seibt[3], J. Schmidt[1], and R. Brendel[1,2]
[1] Institute for Solar Energy Research Hamelin (ISFH), Am Ohrberg 1, 31860 Emmerthal, Germany
[2] Institute for Solid State Physics, Leibniz University Hanover, Appelstr. 2, 30167 Hanover, Germany
[3] IV. Physical Institute, Georg-August University Göttingen, Friedrich-Hund-Platz 1, 37077 Göttingen, Germany

ABSTRACT: Using aluminum oxide (Al$_2$O$_3$) films deposited by atomic layer deposition, the dominant passivation mechanisms at the Si/Al$_2$O$_3$ interface, as well as the chemical composition of the interface region, are investigated. The excellent surface passivation quality of thin Al$_2$O$_3$ films is predominantly assigned to a high negative fixed charge density of $Q_f = -(4 \pm 1) \times 10^{12}$ cm^{-2}, which is located within 1 nm of the Si/Al$_2$O$_3$ interface and virtually independent of layer thickness. A deterioration of the passivation quality for ultrathin Al$_2$O$_3$ layers is explained by a strong increase of the interface state density, presumably due to an incomplete reaction of the TMA molecules during the first ALD cycles. A high oxygen-to-aluminum atomic ratio resulting from the incomplete adsorption of the TMA molecules is suggested as a possible source of the high negative charge density Q_f at the Si/Al$_2$O$_3$ interface.
Keywords: Silicon, Surface Passivation, Al$_2$O$_3$

1 INTRODUCTION

Atomic layer deposition (ALD) of aluminum oxide films has recently attracted large interest due to its excellent potential for highly efficient and homogeneous surface passivation of crystalline silicon [1-4]. Two complementary contributions to a reduction of the surface recombination velocity can be identified: *(i)* a reduction of the density of electronic surface states (chemical passivation), and *(ii)* a reduction of the electron or hole concentration near the surface, e.g. by an internal electrical field (field-effect passivation). In our contribution we investigate the role of both passivation mechanisms at the Si/Al$_2$O$_3$ interface. Figure 1 shows effective lifetimes τ_{eff} measured at an injection density of $\Delta n = 10^{15}$ cm^{-3} on 1.5 Ωcm *p*-type FZ-Si wafers passivated by Al$_2$O$_3$ films deposited by plasma and thermal ALD, respectively. Since a deterioration of the otherwise excellent surface passivation quality is observed for ultrathin Al$_2$O$_3$ layers with a thickness < 5 nm for plasma-assisted ALD and < 10 nm for thermal ALD, we mainly focus on the thickness dependence of the interface properties, i.e. passivation quality and chemical composition of the aluminum oxide film.

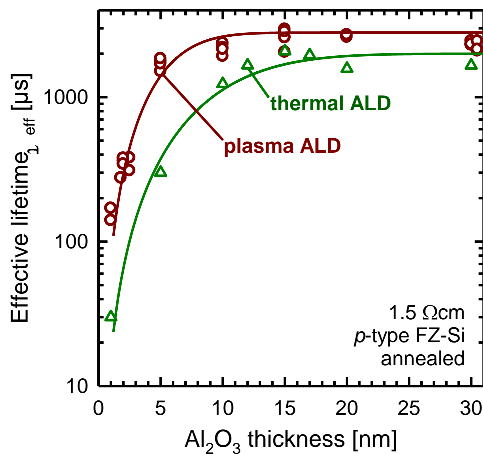

Fig. 1: Effective lifetime τ_{eff} at an injection density $\Delta n = 10^{15}$ cm^{-3} measured on 1.5 Ωcm *p*-type FZ-Si passivated by Al$_2$O$_3$ films of varying thickness, deposited by plasma and thermal ALD.

Industrial application of Al$_2$O$_3$ deposited by ALD is hampered by the low deposition rate of less than 2 nm/min. Scaling current laboratory-type ALD reactors to industrial manufacturing demands and developing high-rate ALD processes is considered to favor the otherwise less studied thermal ALD process over plasma-assisted ALD. Therefore, differences between these two ALD variants – plasma-assisted and thermal ALD – are addressed in this contribution.

2 ELECTRONIC INTERFACE PROPERTIES

2.1 *Fixed charge density and interface state density of ultrathin Al$_2$O$_3$ films*

The contribution of a field-effect passivation to the excellent surface passivation quality compared to a chemical passivation is investigated as a function of Al$_2$O$_3$ film thickness. All lifetime measurements were performed on 1.3 to 1.5 Ωcm *p*-type FZ-Si wafers passivated on both sides by identically deposited Al$_2$O$_3$ films. The wafers have a thickness of 300 µm and were laser-cut in 2.5 × 2.5 cm^2 pieces. The passivation layers were deposited by both plasma-assisted and thermal ALD, and the layer thickness varies from 1 nm to 32 nm. All samples were annealed for 15 min (10 min for layers below 5 nm) at 425 °C in a nitrogen atmosphere to activate the passivation.

The fixed charge density in the Al$_2$O$_3$ films was extracted by Corona charge analysis [5] of the described lifetime samples. The effective carrier lifetimes τ_{eff} were determined by photoconductance decay (PCD) measurements, using a Sinton Instruments lifetime tester, at an injection density of $\Delta n = 10^{15}$ cm^{-3} as a function of Corona charge density Q_C deposited on both wafer surfaces. The effective surface recombination velocity is then calculated from the measured τ_{eff} values by the following equation [6]:

$$S_{eff} = \sqrt{D\left(\frac{1}{\tau_{eff}} - \frac{1}{\tau_b}\right)} \cdot \tan\left(\frac{W}{2}\sqrt{\frac{1}{D} \cdot \left(\frac{1}{\tau_{eff}} - \frac{1}{\tau_b}\right)}\right), \quad (1)$$

where D is the electron diffusion constant, W is the wafer thickness and τ_b is the bulk lifetime, which was assumed

to be equal to the intrinsic lifetime following the empirical parameterization by Kerr and Cuevas [7]. The commonly employed approximation $S_{eff} = W/(2\cdot\tau_{eff})$ for low S_{eff} values does not apply in our case, since very high surface recombination velocities can be encountered for a full compensation of the field-effect passivation during a Corona charge measurement [6].

A maximum of the effective surface recombination velocity S_{eff} occurs for flat-band conditions, where the fixed charge density Q_f in the Al_2O_3 layer is compensated by the deposited Corona charge density Q_c. Analysis of the effective SRV S_{eff} as a function of Corona charge density Q_c hence allows an estimate of both the fixed charge density Q_f and the level of chemical passivation, as given by the SRV parameter S_0 for zero net charge. Comparing surface recombination velocity parameters S_0 obtained from a Corona charge analysis with a detailed capacitance-voltage (C-V) analysis of the interface state density D_{it} allows a scaling of the extracted S_0 parameters to an interface state density D_{it}.

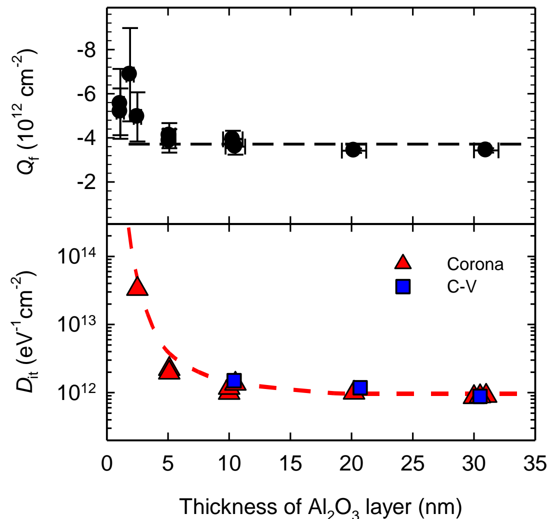

Fig. 2: Fixed charge density Q_f (top graph) and interface state density D_{it} (bottom graph) as determined by Corona charge (red triangles) and capacitance-voltage (blue squares) analysis of Al_2O_3 films deposited by plasma-assisted ALD. The sample with an Al_2O_3 thickness of 30 nm was used to scale the S_0 values obtained by Corona charge analysis to the interface state density D_{it} obtained from the C-V measurements. The dashed lines are guides to the eye.

Figure 2 shows both the fixed charge density Q_f and the interface state density D_{it} for a wide range of Al_2O_3 film thickness values. The ultralow surface recombination velocities routinely obtained on *p*- and *n*-type silicon are predominantly attributed to a strong field effect passivation caused by a high negative fixed charge density of $Q_f = -(4 \pm 1) \times 10^{12}$ cm^{-2} in the Al_2O_3, which is consistent with results published earlier by other authors [2, and references therein]. The apparent rise in Q_f for very thin Al_2O_3 films might be due to calibration errors for ultrathin Al_2O_3 films during the Corona charge experiment. The total amount of deposited Corona charge, as well as the dielectric constant ε_r, are determined by calibrating the increase in deposited Corona charge on a sample of known ε_r and measuring the change of surface potential of the Al_2O_3 layer with a Kelvin probe. However, leakage currents might start to play a role for ultrathin Al_2O_3 films, reducing the total amount of Corona charge remaining on the sample surface. Consequently, the fixed charge density Q_f in the ultrathin films is expected to be closer to the lower bound of the error margin. Taking this into consideration, we find the same high negative fixed charge density of $Q_f = -(4 \pm 1) \times 10^{12}$ cm^{-2} for all samples from 1 nm to 32 nm thickness, which indicates that the negative charges are located within 1 nm of the interface. Consequently, even ultrathin Al_2O_3 films of 1 nm thickness profit from the high level of field-effect passivation, enabling surface recombination velocities $S_{eff} < 100$ cm/s at $\Delta n = 10^{15}$ cm^{-3} on these samples.

The limiting factor for the application of ultrathin passivation layers of Al_2O_3 is their reduced level of chemical passivation. An interface state density $D_{it} = (1.0 \pm 0.2) \times 10^{12}$ eV^{-1}cm^{-2} is measured for the Si/Al_2O_3 interface for Al_2O_3 films down to ~10 nm, which significantly increases for ultrathin layers and explains very well the deterioration of the effective lifetime τ_{eff} with decreasing film thickness observed in Fig. 1. For ultrathin layers of less than 3 nm no significant level of chemical passivation was observed and lifetimes below 5 µs, corresponding to $S_{eff} > 10^4$ cm/s, were measured at $\Delta n = 10^{15}$ cm^{-3} for zero net charge $Q_f + Q_C = 0$. However, due to the strong field-effect passivation caused by the high negative charge density Q_f, effective surface recombination velocities $S_{eff} < 100$ cm/s at $\Delta n = 10^{15}$ cm^{-3} are obtained on the same samples prior to the deposition of Corona charges, in good agreement with results published earlier [8,9].

2.2 *Charge distribution at the interface*

Our measurements indicate similar fixed charge densities for plasma-assisted and thermal ALD, respectively, and S_0 values are found to be lower in Al_2O_3 films deposited by thermal ALD, although plasma-assisted ALD is usually superior in obtaining highest effective lifetimes [10]. A plot of the surface recombination velocity S_{eff} as a function of deposited

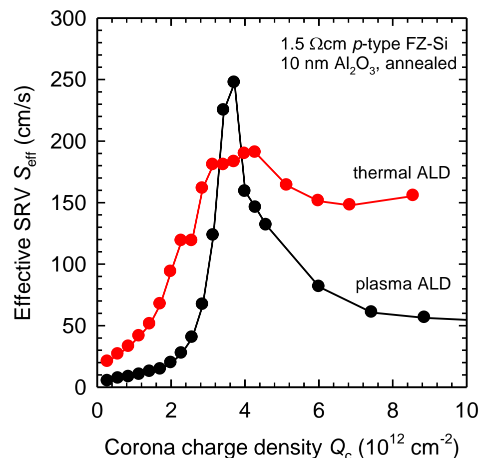

Fig. 3: Effective surface recombination velocity S_{eff} measured at an injection density of $\Delta n = 10^{15}$ cm^{-3} as a function of deposited Corona charge density Q_c for two Al_2O_3 films deposited by plasma and thermal ALD, respectively.

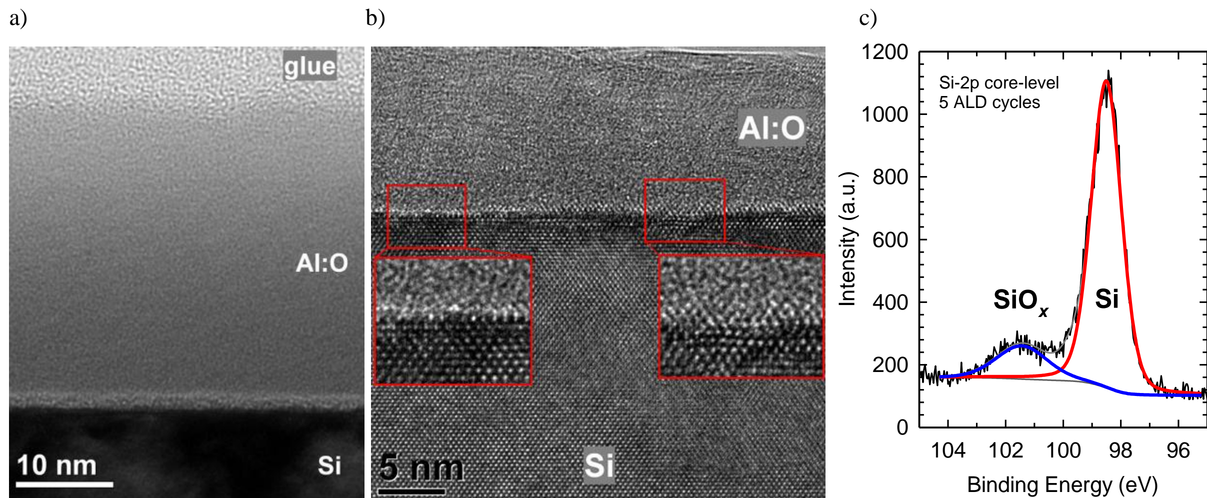

Fig. 4: (a) TEM image of a 30 nm thick Al_2O_3 layer deposited by plasma-assisted ALD. The Al_2O_3 layer has been annealed for 15 min at 425 °C. (b) High-resolution TEM image of the same Al_2O_3 layer. The insets show a magnification of the interface region at the atomic scale. (c) Si-2p core-level peak recorded by XPS on a sample exposed to 5 ALD process cycles. The distinct double-peak structure corroborates a partial oxidation of the Si/Al_2O_3 interface.

Corona charge density Q_C is shown in Fig. 3 for an annealed 10 nm Al_2O_3 layer deposited on 1.5 Ωcm *p*-type FZ-Si. Two major differences between samples passivated by thermal and plasma-assisted ALD are identified:

(i) The peak of the effective surface recombination velocity S_{eff} around $Q_c = - Q_f$ is broader for samples passivated by thermal ALD than in the case of plasma-assisted ALD. The broader shape of the peak can be explained by a spatially inhomogeneous charge distribution in the thermal ALD samples, whereas the fixed charges in the Al_2O_3 films deposited by plasma-assisted ALD are considered to be spatially more homogeneous compared to the inhomogeneity of the deposited Corona charge, resulting in a sharper $S_{eff}(Q_c)$ peak. As a consequence, the level of chemical passivation achieved by thermal ALD cannot be directly accessed by Corona charge measurements, since a locally non-zero charge density remains even for a deposited Corona charge density equal to the mean absolute fixed charge density $|\langle Q_f \rangle|$.

(ii) In the regimes where the total charge density $Q_f + Q_c$ is sufficiently large to provide an effective field-effect passivation, the measured effective surface recombination velocities S_{eff} are larger for thermal ALD than is the case for plasma-assisted ALD, indicating a lower chemical passivation. We propose that a higher hydrogen concentration [11] in the thermal ALD layers leads to a deterioration of the crystalline quality beneath the interface, resulting in an increased recombination rate originating from the space charge region [12] which extends into the degraded volume.

3 CHEMICAL COMPOSITION OF THE INTERFACE

A thin (1 nm – 2 nm) layer of SiO_x at the Si/Al_2O_3 interface had previously been reported and was considered to play an important role in the passivation of silicon surfaces by Al_2O_3 layers [13]. In order to directly verify the presence of such an interfacial SiO_x layer, we examine the Si/Al_2O_3 interface by cross-sectional transmission electron microscopy (TEM). The Al_2O_3 layer under investigation has a thickness of 30 nm and has been deposited by plasma-assisted ALD on a shiny-etched 1.5 Ωcm *p*-type FZ-Si wafer and subsequently annealed for 15 min at 425 °C in a nitrogen atmosphere. Figure 4(a) shows a TEM image of the Si/Al_2O_3 interface. Details of the surface morphology are given by a high-resolution TEM image in Fig. 4(b). A bright feature at the Si/Al_2O_3 interface – which might have been mistakenly interpreted as a thin interfacial SiO_x film of a few nanometers – is indeed revealed by the TEM images in Fig. 4. However, a comparison of the thickness of this feature for different magnifications clearly marks it as an edge diffraction artifact. Therefore, the TEM images clearly refute the presence of a noticeable interfacial SiO_x layer with a thickness of the order of a few nanometers, although they do not exclude the presence of a few monolayers of SiO_x at the interface.

A thin interfacial SiO_x layer of the order of 2 – 3 monolayers is indeed identified by X-ray photoelectron spectroscopy (XPS). A pronounced energy-resolved silicon signal can only be resolved for thin Al_2O_3 films below a few nanometers, where scattering of photoelectrons originating from the Si/Al_2O_3 interface is negligible. On these samples the silicon core-level peaks show a distinct double-peak structure, as exemplified by the Si-2p core-level for 5 ALD cycles of Al_2O_3 shown in Fig. 4(c). This clearly indicates an oxidation of the silicon surface, forming a SiO_x interface between the silicon and aluminum oxide. The thickness of the interfacial SiO_x is estimated by the relative contribution of the Si–Si and Si–O signals to the Si-2p double-peak to be 2 or 3 monolayers.

A thickness-dependent analysis of the chemical composition is presented here by varying the number of ALD cycles for the deposition of the Al_2O_3 films (0, 1, 5, 30 and 125 cycles). In addition, the sample preparation (HF dip prior to deposition/no HF dip) and post-deposition anneal (annealed in forming gas/not annealed) are varied.

For samples coated with only one ALD cycle no aluminum is detected at all, indicating that at least one

"starting cycle" is required to generate a suitable nucleation surface for the ALD process. In addition, a negligible oxygen concentration is detected for the samples which received an HF dip prior to deposition.

After 5 ALD cycles an aluminum-to-oxygen ratio of 1:10 is calculated from the integrated intensities of the Al-2p and O-1s peaks. Subtracting the oxygen contribution of the interfacial SiO_x layer yields an Al:O ratio of 1:8, which is far from the stoichiometric 2:3 atomic ratio. The Al:O ratio increases for thicker layers, yielding ratios of 2:7.4 for 30 cycles and 2:5.6 for 125 cycles, respectively. We conclude that in the native state or after an HF dip the functional surface groups on the silicon wafer are not optimal for an adsorption of the TMA precursor molecules, which leads to an incomplete reaction of the TMA and, consequently, an increased relative oxygen concentration at the interface. The incomplete ALD process during the first cycles might explain the increased interface state density for ultrathin Al_2O_3 films, since deposition might start by formation of nucleation islands, leaving parts of the silicon substrate unpassivated. Furthermore, structural defects and dangling bonds introduced during the beginning of the ALD process might be healed at a later state, e.g. by hydrogen passivation during the thermal post-deposition anneal, if a sufficiently large "bulk" of Al_2O_3 is present in thicker layers.

Since no clear XPS double-peak structures are resolved for the aluminum and oxygen peaks, both species are assumed to be present in only one charge state. Consequently, a single atomic species cannot sufficiently well explain the origin of the high negative fixed charge density. We propose the high oxygen-to-aluminum ratio caused by the incomplete ALD process during the first cycles as a candidate for the origin of the high negative charge density at the interface.

Remarkably, already after 5 ALD cycles neither the thickness of the SiO_x interface nor the Al:O ratio for a given thickness depends on the post-deposition anneal or an HF dip prior to deposition.

4 CONCLUSIONS

The physical mechanisms responsible for the excellent surface passivation quality provided by Al_2O_3 films grown by ALD were investigated. Both field-effect passivation due to a high negative fixed charge density of $Q_f = -(4 \pm 1) \times 10^{12}$ cm^{-2} and chemical passivation due to a moderate interface state density of $D_{it} = (1.0 \pm 0.2) \times 10^{12}$ eV^{-1}cm^{-2}, which deteriorates for thin layers below ~10 nm, were identified by Corona charge and capacitance-voltage measurements. The negative charges responsible for the strong field-effect passivation were shown to be located within 1 nm of the Si/Al_2O_3 interface, although a spatially inhomogeneous charge distribution was found for layers deposited by thermal ALD. For ultrathin Al_2O_3 films the density of interface states was shown to increase significantly, presumably due to an incomplete reaction of the TMA precursor molecules during the first few cycles of the ALD process, where the functional groups at the silicon surface are not optimal for an adsorption of the TMA precursor molecules. However, due to the high fixed charge density responsible for the excellent level of field-effect passivation, low surface recombination velocities $S_{eff} <$ 100 cm/s at $\Delta n = 10^{15}$ cm^{-3} were measured on 1.5 Ωcm *p*-type FZ-Si samples passivated by Al_2O_3 films of only 1 nm thickness.

The structural and chemical composition of the Si/Al_2O_3 interface was studied by XPS and high-resolution TEM analysis. XPS measurements revealed that 2 – 3 monolayers of an interfacial SiO_x film form at the Si/Al_2O_3 interface. In addition, a high concentration of oxygen and, as a consequence, a significant deviation from stoichiometry in the Al_2O_3 films was evidenced near the interface. The high oxygen-to-aluminum atomic ratio near the interface was proposed to be a likely candidate for the origin of the high negative fixed charge density.

ACKNOWLEDGEMENT

Funding was provided by the State of Lower Saxony and the German Ministry for the Environment, Nature Conservation and Nuclear Safety (BMU) under contract number 0325050 ("ALD").

REFERENCES

[1] G. Agostinelli, A. Delabie, P. Vitanov, Z. Alexieva, H. F. W. Dekkers, S. De Wolf, and G. Beaucarne, *Solar Energy Materials and Solar Cells*, **90**, 3438 (2006)

[2] B. Hoex, J. J. H. Gielis, M. C. M. van de Sanden, and W. M. M. Kessels, *J. Appl. Phys.*, **104**, 113703 (2008)

[3] J. Schmidt, A. Merkle, R. Brendel, B. Hoex, M. C. M. van de Sanden, and W. M. M. Kessels, *Progr. Photovolt.*, **16**, 461 (2008)

[4] J. Benick, A. Richter, M. Hermle, and S. W. Glunz, *Phys. Stat. Sol. RRL*, **3**, 233 (2009)

[5] S. Dauwe, J. Schmidt, A. Metz, and R. Hezel, *Proc. 35th IEEE Photovoltaic Spec. Conf.*, New Orleans, LA, p. 162 (IEEE, New York, 2002)

[6] A. B. Sproul, *J. Appl. Phys.*, **76**, 2851 (1994)

[7] M. J. Kerr, and A. Cuevas, *J. Appl. Phys.*, **91**, 2473 (2002)

[8] J. Schmidt, B. Veith, and R. Brendel, *Phys. Stat. Sol. – RRL*, **3**, 287 (2009)

[9] G. Dingemans, R. Seguin, P. Engelhart, M. C. M. van de Sanden, and W. M. M. Kessels, *Phys. Stat. Sol. – RRL*, **4**, 10 (2010)

[10] J. Schmidt, B. Veith, F. Werner, D. Zielke, and R. Brendel, *Proc. 35th IEEE Photovoltaic Spec. Conf.*, Honolulu, HI, in press (2010)

[11] G. Dingemans, M. C. M. van de Sanden, and W. M. M. Kessels, *Electrochem. and Solid-State Lett.*, **13**(3), H76 (2009)

[12] S. Steingrube, P. P. Altermatt, D. Zielke, F. Werner, J. Schmidt, and R. Brendel, *Proc. 25th EUPVSEC*, Valencia, Spain (2010)

[13] B. Hoex, S. B. S. Heil, E. Langereis, M. C. M. van de Sanden, and W. M. M. Kessels, *Appl. Phys. Lett.*, **89**, 042112 (2006)